In-Situ Atomic Force Microscopy of Polyethylene Crystallization. 1. Crystallization from an Oriented Backbone

J. K. Hobbs,* A. D. L. Humphris, and M. J. Miles

H. H. Wills Physics Laboratory, Tyndall Avenue, Bristol BS8 1TL, UK

Received March 13, 2001; Revised Manuscript Received May 16, 2001

ABSTRACT: Atomic force microscopy has been used to image the crystallization of polyethylene shish kebab crystals in situ, in real time, with nanometer resolution. Images of the extended chain backbone and overgrowth and subsequent interdigitation of lamellae have been obtained. Direct observation of the interdigitation process shows that the lamellae sometimes change direction so as to avoid meeting, providing evidence of the influence of a growing lamella on its surrounding environment. The growth rates of individual lamellae as they grow from the backbone have been measured and found to vary both with time and from lamella to lamella, in direct contradiction to many theories of polymer crystallization. These data, taken from the first AFM experiments to obtain such high resolution at such a high temperature during a process, provide a significant advance in the capability of AFM to increase our understanding of polymer crystallization.

Introduction

The crystallization of synthetic polymers, and of polyethylene in particular, has been a subject of intensive study for more than 40 years.[1−4] However, many questions remain unanswered, and the models that have been developed frequently fail to explain new observations. One of the most significant gaps in our knowledge is due to an inability to obtain real space information on submicron length scales, during the process of crystallization, without significantly damaging the sample. Atomic force microscopy offers the possibility of following the process of crystallization, in situ, in real time, with nanometer resolution. In this series of papers we present the initial results of a study of the crystallization behavior of polyethylene using this relatively new technique. This first paper deals exclusively with the crystallization of oriented structures as the orientation removes some of the possibilities for confusion that occur when more usual crystallization conditions are followed.

The crystallization of polyethylene from melts or solutions that have undergone extensional flow has been studied for many years.[5−9] The characteristic morphologies formed by this processing route are a largely extended chain backbone, with platelike lamellar overgrowths, leading the name “shish kebab” crystal to be adopted. The primary differences between solution and melt crystallization is a considerably higher density of the overgrowths in the case of melt growth, frequently concealing the underlying oriented backbone. It is now well established that the initial morphology of an extended chain backbone is formed due to the action of the imposed extensional flow field which has the largest effect on the longest molecules, with further growth of the backbone possibly occurring by a self-propagating method.[10,11] This backbone then provides a high-quality, nucleating surface for further crystallization in the “normal” chain folded manner. If the extensional flow was imposed at a high temperature, secondary crystallization may only become active once the material has been cooled to a sufficiently low temperature to allow appreciable growth rates of the relatively thin lamellae.

As well as being of interest in its own right, and for commercial reasons, shish kebab crystallization has also been studied because of the insights it can give into lamellar growth.[12] By constraining the lamellae to grow parallel to each other, and perpendicular to a predetermined direction (the direction of extension), the final morphology is controlled, and some new insights into polymer growth can be obtained.

Atomic force microscopy has been increasingly used over recent years to study processes in synthetic polymers, in particular crystallization and melting.[13−20] Recently, these studies have been extended to include the following of processes at progressively higher temperatures,[18−20] to the extent that the crystallization and melting of many commercial polymers can now be followed. The current paper, building upon our previous work on polyethylene shish kebabs,[20] follows the crystallization from the extended chain backbone with unprecedented resolution, in situ, in real time.

Experimental Method

A sharp polyethylene fraction was used, supplied by the National Bureau of Standards (M_w 119 600, M_w/M_n 1.19). A 1% suspension of the polymer in *p*-xylene was prepared by dissolving for 20 min at 120 °C and quenching to room temperature. A drop of the suspension was then placed on a glass coverslip on a hot bench at 150 °C and held in the melt for 2 min. The resulting thin film was quenched to room temperature. This film was remelted on a Linkam hot stage at 160 °C for 2 min and cooled to 145 °C.

Two different methods were used for orienting the melt. In some cases a razor blade was dragged across the sample in order to cause oriented crystallization in the melt. When this process was observed using an optical microscope, it was clear that the melt started to crystallize as soon as the blade was brought into contact with the melt, due to the drop in temperature that this caused. A highly oriented birefringent area was formed where the razor blade had sheared and extended the melt. As soon as the razor blade was removed, the unoriented regions remelted, but the high birefringence remained in the oriented part of the film. In later studies a different method was used which prevented the sample from fully crystallizing and then remelting before it could be

* Corresponding author. Tel 44 (0)117 9288747; Fax 44 (0)117 9255624; E-mail jamie.hobbs@bristol.ac.uk.

10.1021/ma0104478 CCC: $20.00
Published on Web 06/26/2001

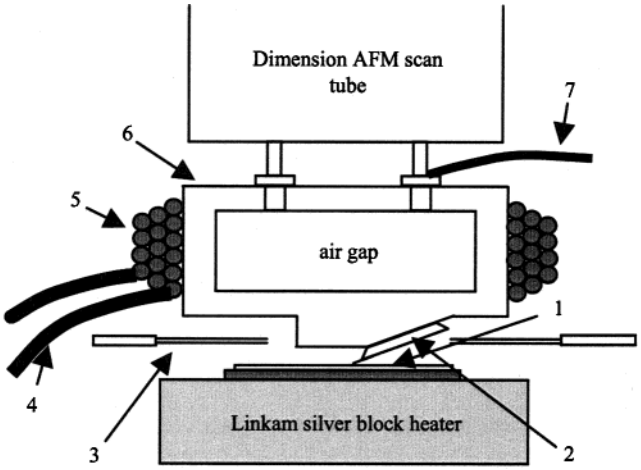

Figure 1. Schematic diagram showing the modified cantilever holder used for some of the experiments: 1, the sample mounted on a glass slide; 2, the cantilever substrate; 3, the aluminum and Kapton heat shield; 4, copper wire from coil to current driver; 5, copper coil; 6, glass cantilever holder; 7, thermocouple.

observed. A second piece of glass was placed on top of the sample before it was heated and, after heating to 160 °C and cooling to 145 °C, was dragged across the surface and removed. This gave highly oriented birefringent regions that were stable at 145 °C but did not result in the more general crystallization of the sample as the whole system was maintained at the elevated temperature.

The Linkam was cooled to 135 °C and then moved into position under the scan tube of a Digital Instruments D3100 AFM. Two different methods were used to protect the piezoelectric crystal from the heat. In initial studies, a sheet of aluminum foil and a sheet of Kapton were placed between the scan tube and the heater, the cantilever projecting through a small hole in these protective sheets. Although this allowed stable imaging of the sample surface, it resulted in the scan tube obtaining temperatures close to its depoling temperature. To allow higher temperatures to be reached, a different method was developed which allowed the scan tube to be more thoroughly insulated from the heater. This device will be described in more detail in a subsequent publication, but the basic principle will be outlined here. A new cantilever holder was made from glass, as shown schematically in Figure 1. The air gap enables a large temperature gradient to be sustained between the heater and the scan tube. As the dither piezo would also be in danger of depoling, this was removed from the system, and the cantilever was oscillated magnetically. A coating of ~70 nm cobalt was evaporated onto the backside of the cantilever, which was then driven magnetically using a small solenoid wrapped around the cantilever holder, in a manner similar to that used frequently for magnetic drive in liquids.[21] Drive currents of approximately 1amp were typically necessary to give the desired amplitude of oscillation. By using this device in conjunction with the heat shield, sample temperatures of upward of 150 °C can be safely accessed.

The accurate measurement of the temperature of the sample surface is influenced by the distance from the heat shield, the alignment of the probe relative to its holder etc., all of which vary from experiment to experiment, making a reliable calibration problematic. The temperature difference between the sample surface and the heater was estimated to be 3.5−7 °C for the experiments reported here. The temperatures quoted in the text are the temperature given on the Linkam and are therefore ~4 °C higher than the estimated sample temperature. When the AFM probe is initially brought into contact with the surface, it takes some time for temperature equilibrium to be reached between the sample and the cantilever system. This process is asymptotic, but it was found that a steady state was approached within a minute or so, with a very gradual increase in surface temperature occurring over longer times, as discussed below. The thermal isolation of the cantilever from the large thermal mass of the scan tube etc., through the use of the novel cantilever holder described above, considerably improves control over this process. The temperature stability after imaging had begun was better than 0.1 °C, as evidenced by clear drift of the sample when temperature changes of this order were introduced by cooling the stage. (Drift due to changes in temperature can be differentiated from drift due to air movements as the former has a particular direction due to the geometry of the heater and the position of the imaged area relative to that geometry.)

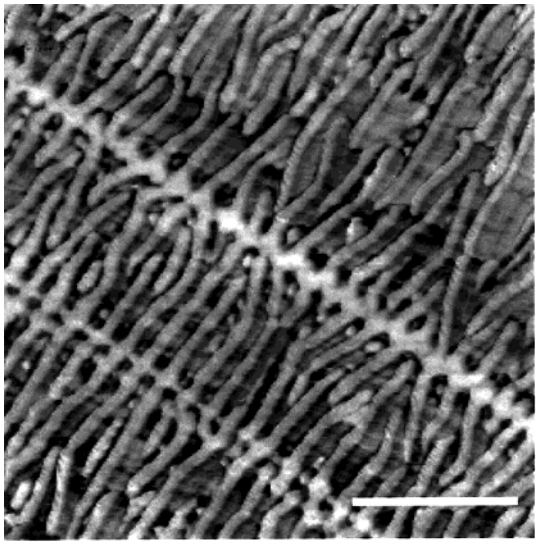

Figure 2. Phase image showing a polyethylene shish kebab structure formed by shearing a sample with a razor blade, taken at room temperature. The gray scale represents a change in phase angle of 70°. The scale bar represents 300 nm.

The AFM was operated in tapping mode, and phase, height, and amplitude images were collected simultaneously. Imaging conditions were maintained so as to just allow the surface to be tracked while maintaining the fast scan rates necessary to follow the process. All images were taken at 256 × 256 pixels.

Results

Figure 2 is a phase image of a typical sheared sample after quenching to room temperature. The individual lamellae can be seen as well as three separate, clearly defined, row nuclei, passing diagonally across the image. The lower two of these nuclei are clearly extended chain or "shish" crystals similar to those found in solution crystallization, while the upper one has been overgrown by lamellae, concealing the backbone. The image quality compares favorably with those obtained by TEM. The sample preparation technique, although crude, provides good examples of the shish kebab morphology, which it is the aim of this work to image.

Figure 3 shows a high-resolution image taken at a temperature of 135 °C, after shearing the melt with a razor blade at 145 °C. The bright area in the top right of the image is the glass substrate; the dark areas are molten polymer. The glass substrate and the polymer, both being hard, elastic materials with a low adhesive interaction with the AFM tip, have a similar phase angle when compared to the soft, adhesive, molten polymer. The film thickness is ~50 nm. The classic shish kebab morphology is visible, with the extended chain backbone and the individual lamellae spaced irregularly along it, lying dormant in the melt at this temperature. The similarity between this morphology and that seen in crystallization in stirred solutions is striking.

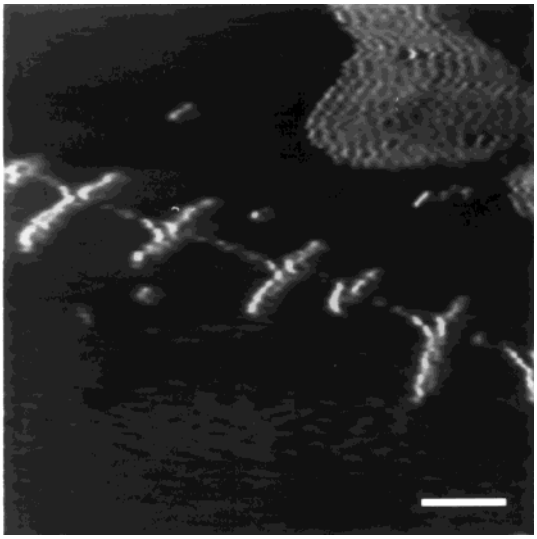

Figure 3. Phase image showing a polyethylene shish kebab structure, taken at a temperature of 135 °C. The bright area in the top right of the image is the glass substrate. The dark areas are amorphous polymer. The gray scale represents a change in phase angle of 60°. The scale bar represents 100 nm.

After observation of the dormant shish kebab at a temperature sufficiently high that further growth of the lamellae did not occur, the sample was slowly cooled and the growth of the lamellae observed. The cooling was carried out at a rate of 0.5 °C/min and held every 0.5 °C to allow observation of both isothermal and nonisothermal crystallization. Figure 4 shows a series of images taken during this slow cooling cycle. The area corresponding to that shown in Figure 3 is marked with a box. Three separate extended nuclei are present in the area imaged, although the backbone itself is only clearly visible in the upper shish kebab. The presence of three shish kebabs in the field of view allows the observation of the interdigitation of the lamellae as they grow. Figure 5 shows a slightly higher resolution series of images taken further along the cooling cycle. Figure 6 shows the last stages of interpenetration of the structure.

Figure 7 shows the same area imaged after cooling to room temperature. This last image is an amplitude image as the phase resonance response of the cantilever had been altered during cooling to room temperature, and it was not possible to significantly alter the experimental setup without risking being unable to find the area previously imaged. In Figure 7, two separate populations of lamellae are present: those that grew at higher temperatures, and were imaged in Figures 4−6, and those that grew on cooling to room temperature and are particularly predominant in the lower right-hand quarter of the image. These latter lamellae are substantially thinner than those that grew at higher temperatures, as expected.

Figure 8 shows a series of images taken during another experiment in which the sample was continuously cooled at 0.5 °C/min from 128.5 °C. This sample had been prepared by shearing with a razor blade. The temperature was lower in this experiment, and hence the growth rate faster, so fewer images were collected during the growth process. In Figure 8 the extended chain backbones cannot be seen, although the growth and interdigitation of the lamellae are visible.

Figure 9 shows another series of images, this time taken during slow isothermal crystallization at a nominal temperature of 131.8 °C. (Comparison between the growth rates measured, and those reported for this material in ref 4, suggest that the true sample temperature in this experiment was 128 °C. However, as the experimental setup differed from experiment to experiment, this cannot be taken as an accurate calibration of the temperature for all the experiments.) This series of images was taken using the magnetically oscillated cantilever method, and the sample was prepared by shearing with a second glass slide. Again, the extended chain backbone is not visible. However, in this experiment, a very large number of images were obtained at constant temperature, allowing the measurement of the growth rates of the individual lamellae. In Figure 9 a very high scan rate was maintained to allow the collection of a large number of consecutive images. This has led to some degradation in image quality, in particular in the tracking of the surface as the tip passes from the lamellae onto the melt, so that some of the surface is not imaged at all. An example of this is arrowed in Figure 9f and can be seen in all of the images in Figure 9 as the dark regions on the right-hand side of the curved lamellae. This failure in tracking also leads to occasional artifacts, in which there appears to be two lamellae next to each other when this is not really the case. An example of such an artifact is arrowed in Figure 9d. To allow these images to be correctly interpreted, while maintaining the fast scan rates that would enable the information to be obtained that we desired, images were collected on both the trace and retrace of each scan line. Figure 10 shows an example of such a pair of images, taken during the same scan. The different direction of scanning can be clearly seen from differences in the tracking artifact seen as the feedback mechanism loses control immediately after passing over the higher lamellae (in particular, those that are curving, arrowed). By comparison of trace and retrace images, it is possible to define the true size of the lamella, and the presence of scan artifacts can be clearly determined. This slight degradation in image quality was felt to be a necessary evil if the desired fast scan rates were to be maintained over this scan area.

Figure 11 shows the growth rates measured over a period of 278 s (that is the distance grown between the third and the twelfth image of the series) near the beginning of the experiment. The lamellae are numbered in Figure 10b. These data were obtained from the trace data. Figure 12 shows the growth rates, measured from the retrace data, of six of the lamellae labeled in Figure 10b. The retrace data were chosen for these measurements, as it is easier to ascertain the exact position of the end of the lamellae and hence get accurate growth rates. (Retrace data were not collected at the beginning of the experiment, but some interesting features of the growth did occur; hence the presentation of some growth rates from the trace data set.) Each rate was measured by taking the change in length of the lamellae over a period of five images (i.e., starting with image one and ending with image five), the time being the time for the initial scan to finish, plus the time for three complete scans, plus the time for the scan to reach the end of the lamella in the fifth scan. It was decided to effectively average the data in this way, as the resolution is insufficiently good compared to the growth rate to allow accurate changes in length to be measured

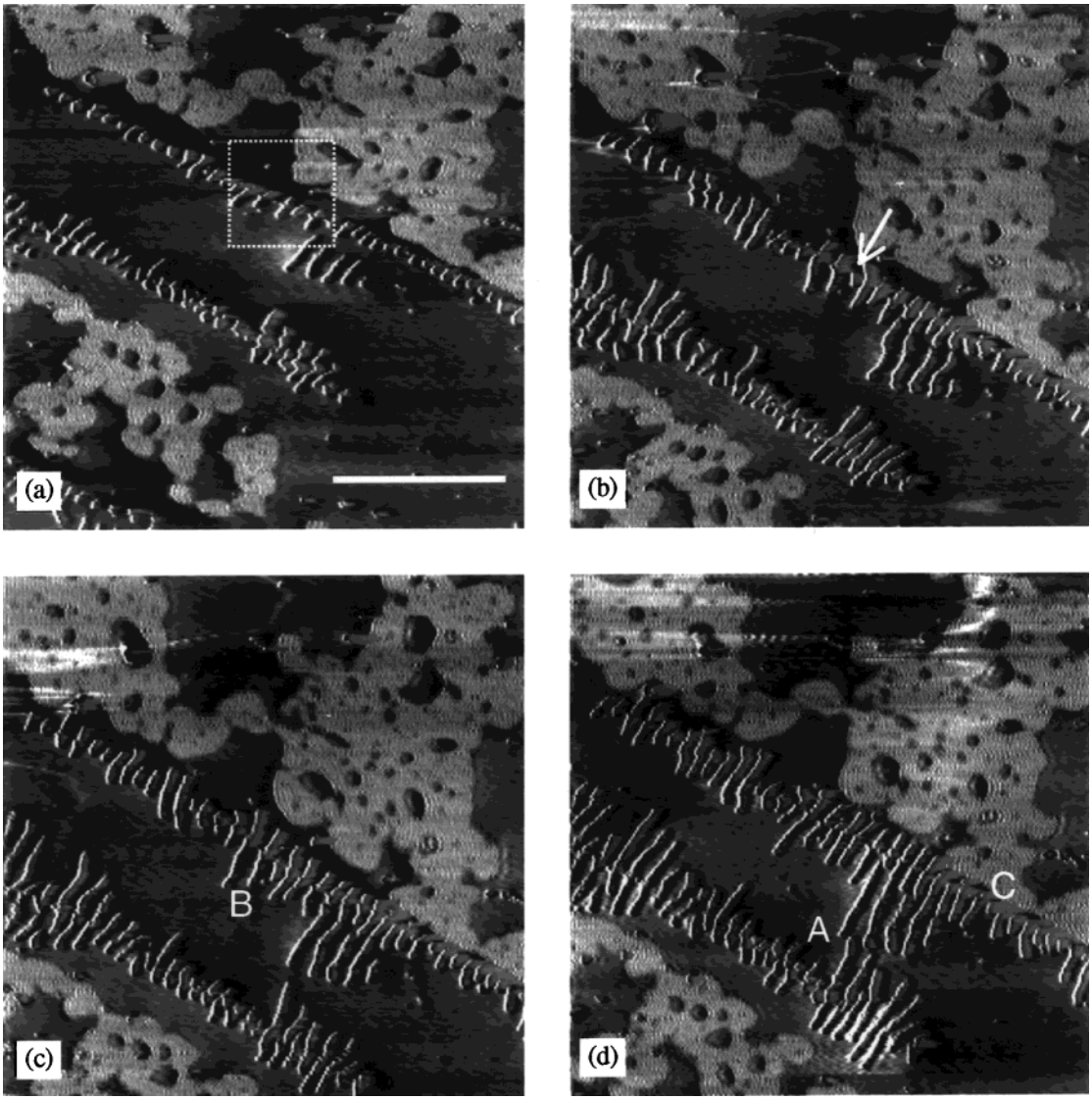

Figure 4. A series of phase images showing the growth of the shish kebab structure. The gray scale represents a change in phase angle of 60°. The scan rate was 3.9 lines/s. The scale bar refers to all the images and represents 1 μm. (a) Taken at 134.5°; the dotted square indicates the area of Figure 2. (b) Taken at 132.5 °C; the arrow indicates a point on the extended chain backbone where a new nucleation event has occurred. (c) Taken at 132.5 °C; the B indicates a lamella that has stopped growing; (d) taken at 132 °C; the A indicates a pair of lamellae that have changed direction to avoid joining, and the C indicates a lamella that lies dormant for the duration of the experiment, as indicated in Figure 6.

between consecutive scans. Thus, each rate is the average growth rate over approximately 124 s, the actual time being slightly different from this because of the change in the position of the lamella tip relative to the top or bottom of the scan. The rates are presented from pairs of images, starting at the tenth image in the series and ending on the 40th. Treating the data in this way is better than the alternative of scanning slower, as slow scanning would lead to a significant difference in the age of different parts of the same image, making measurement of lengths and positions difficult.

Discussion

The results presented above provide a wealth of new information both on shish kebab crystallization and on the crystallization of polyethylene lamellae in general. In what follows we will discuss these data with an emphasis on the new insights that can be obtained into polymer crystallization. The discussion of the novel way of constructing the heating stage/cantilever holder will be left to a subsequent publication.[22] However, there are some features of the imaging that affect all of the data and will be discussed first.

Interpretation of Images and the Effect of Temperature and Fast Scanning. The majority of the data presented here have used fast scan speeds and have been taken at high temperatures. Both of these factors can have a detrimental impact on image quality. At high temperatures the effects of air movements on the stability of the cantilever are significantly amplified. These lead to occasional drift in the images or very low-frequency noise. The images shown in Figure 5 show several clear examples of this noise. It is characterized by the shearing of the image over a number of scan lines. For instance, in Figure 5d, in the area between the two parallel dotted lines, all of the lamellae appear to have bent toward the vertical. As this feature occurs simultaneously across the whole of the width of the image, it is clearly an artifact. Thus, kinks etc. in lamellae must be treated with caution and are unlikely to be real if they are not there in subsequent images or if neighboring lamellae kink at the same time on the

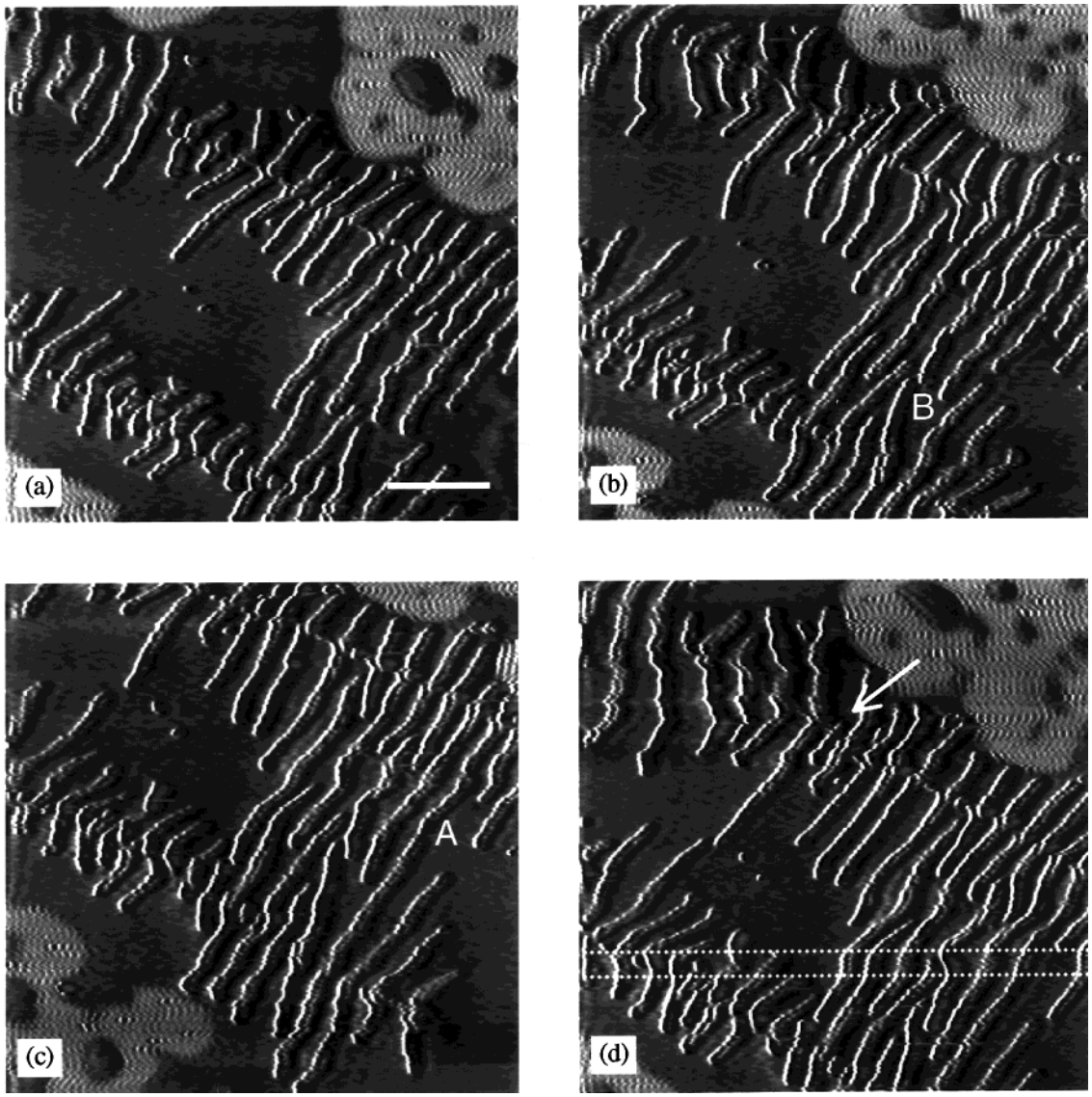

Figure 5. A series of phase images taken at higher resolution, showing the further growth of the shish kebab structure imaged in Figures 3 and 4. The gray scale represents a change in phase angle of 60°. The scan rate was 6.1 lines/s. The scale bar refers to all the images and represents 300 nm. (a) Taken at 132 °C. (b) Taken at 131.5 °C; the B indicates a pair of lamellae that have changed direction to avoid joining. (c) Taken at 131 °C; the A indicates a pair of lamellae that have joined. (d) Taken at 130.5 °C; the arrow indicates a point on the extended chain backbone where a new nucleation event has occurred, and the dotted lines show the distorting effect of drift, in which all the lamellae on a series of scan lines are deformed.

same horizontal line. These problems are particularly prevalent in the first experiment, Figures 3−6, as better shielding in later experiments caused a significant improvement in stability.

In AFM it is necessary to bring a sharp tip into contact with the surface, and therefore a cantilever, cantilever substrate, substrate holder, etc. must all be in close proximity with the surface. In the setup used here, the heater and the cantilever holder start at a different temperature, as the cantilever holder is not actively heated. This will therefore change the temperature of the surface in the region around the area being imaged, and some new temperature equilibrium will be reached. The use of the novel cantilever holder reduces this effect somewhat as the cantilever is more isolated from the large thermal mass of the scan tube that is, by necessity, at a lower temperature. The issue is whether this reduction in temperature is a local effect, centered on the location of the tip, or whether reduction in temperature occurs over a wider area. By taking occasional large scans (30 μm), we have observed that the morphology and extent of growth are not different in the small areas that we are imaging compared with its immediate vicinity (that is the rest of the scan). The presence of the AFM probe is not significantly altering the crystallization behavior.

In all the data presented, very fast scan rates were used in order to allow processes to be followed. This has two effects on image quality. In some areas the surface is not tracked properly, particularly after the cantilever has passed over a high or stiff object, such as a lamella. Examples of this can be seen down the right-hand side of the lamellae in Figure 4b. Although this could have been avoided by changing the scan parameters, it would have necessitated either slower scanning, removing the point of the experiment, or harder tapping, which would have damaged the sample surface. Thus, as the actual lamellae are still clearly visible, we consider this degradation in image quality to be a necessary evil. Similarly, the oscillations in magnitude in the phase signal when imaging the hard glass substrate, which could be removed by slower scanning, do not signifi-

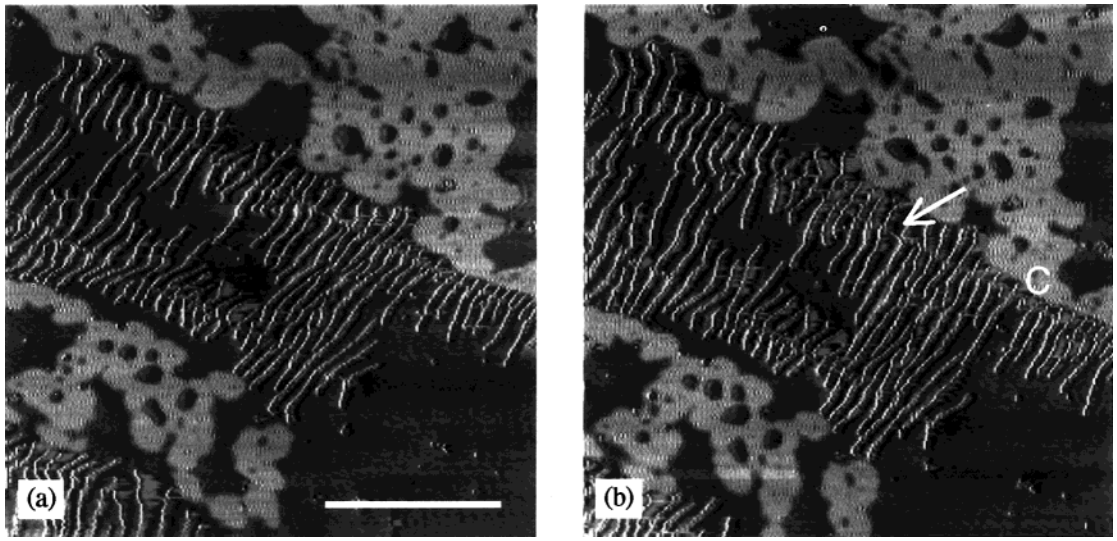

Figure 6. A pair of phase images showing the later stages of growth of the shish kebab structure imaged in Figures 3−5. The gray scale represents a change in phase angle of 60°. The scan rate was 3.0 lines/s. The scale bar refers to both the images and represents 1 μm. (a) Taken at 130.5 °C. (b) Taken at 130 °C; the arrow shows a gap of ∼70 nm where no nucleation has occurred on the backbone, and the C indicates a lamella that lies dormant for the duration of the experiment, as seen by comparison with Figure 4d.

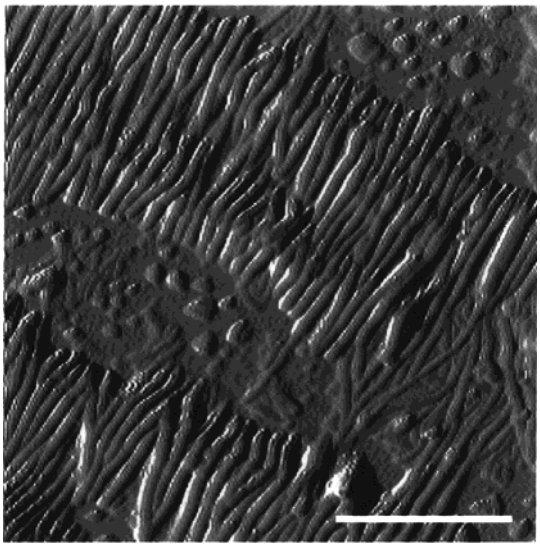

Figure 7. An amplitude image, taken at room temperature, showing the same area as imaged during crystallization in Figures 3−6. The gray scale represents a change in amplitude of 0.5 V. The scale bar represents 1 μm.

cantly impede the interpretation of the image.

As AFM is a surface technique, there is some possibility of misinterpreting the data, especially when measuring rates. We discussed this in a previous paper,[13] but in the current work it is possible to be more confident in our interpretation due to the nature of the morphology under examination. The growth is that of continuous lamellae, growing from a shish nucleus in a thin film. It is unlikely that there is significantly faster growth beneath the surface, as the substrate has no nucleating effect. It is also possible that the growth behavior is influenced by the thickness of the film. It is well-known that in very thin films, once the thickness is of the same order as the lamellar thickness and/or molecular size, the growth morphology changes and diffusion effects become more significant. Most of the data presented here do not fall into that category, with the exception of the growth around the edges of the film imaged in Figures 3−7, as discussed below. The use of relatively thin films was necessitated by the desire to avoid a significant population of extended nuclei at different levels within the melt that could grow up and impinge upon the observation of crystallization, at the same time as allowing two adjacent extended nuclei to be observed at lamellar resolution and hence the imaging of the interdigitation of the lamellae.

Nucleation and the Amorphous Thickness. Close examination of Figure 3 shows that where the lamellae are attached to the backbone they are considerably thicker than once they have penetrated some distance into the melt. Either the initial nucleation on the extended chain backbone is thicker than the subsequent growth of the crystal, or else where the lamella is attached to the extended chain "substrate", the chains are able to thicken rapidly, resulting in a gradual transition in thickness. It has been suggested[6] that the lamellae that are stable at the highest temperatures are those that incorporate chains that are also incorporated in the backbone. This could also lead to somewhat thicker crystals being able to grow.

The first series of images, shown in Figures 3−7, provides two examples of the nucleation of new lamellae on the extended chain backbone, as already briefly discussed in ref 20. This is the first time that such a secondary nucleation process onto the extended chain substrate has been observed, with exciting possibilities for gaining a new understanding of this process. The nucleation events occurred during cooling rather than isothermally in this experiment. The nucleation of new lamellae occurred between Figures 4a,b and 5c,d, and the newly nucleated lamellae are arrowed in Figures 4b and 5d.

Perhaps more interesting is the lack of nucleation in a number of quite large expanses of the backbone. A further insight into this phenomenon can be gained by observing the growth of the lamellae. As lamellae grow, there is a wide amorphous region on each side of them. There are also gaps along the backbone where no lamellae nucleate: for instance, in Figure 6b, after all the nucleation had occurred, there is still a gap on the backbone of approximately 70 nm, as indicated with an arrow. Even on cooling to room temperature the neigh-

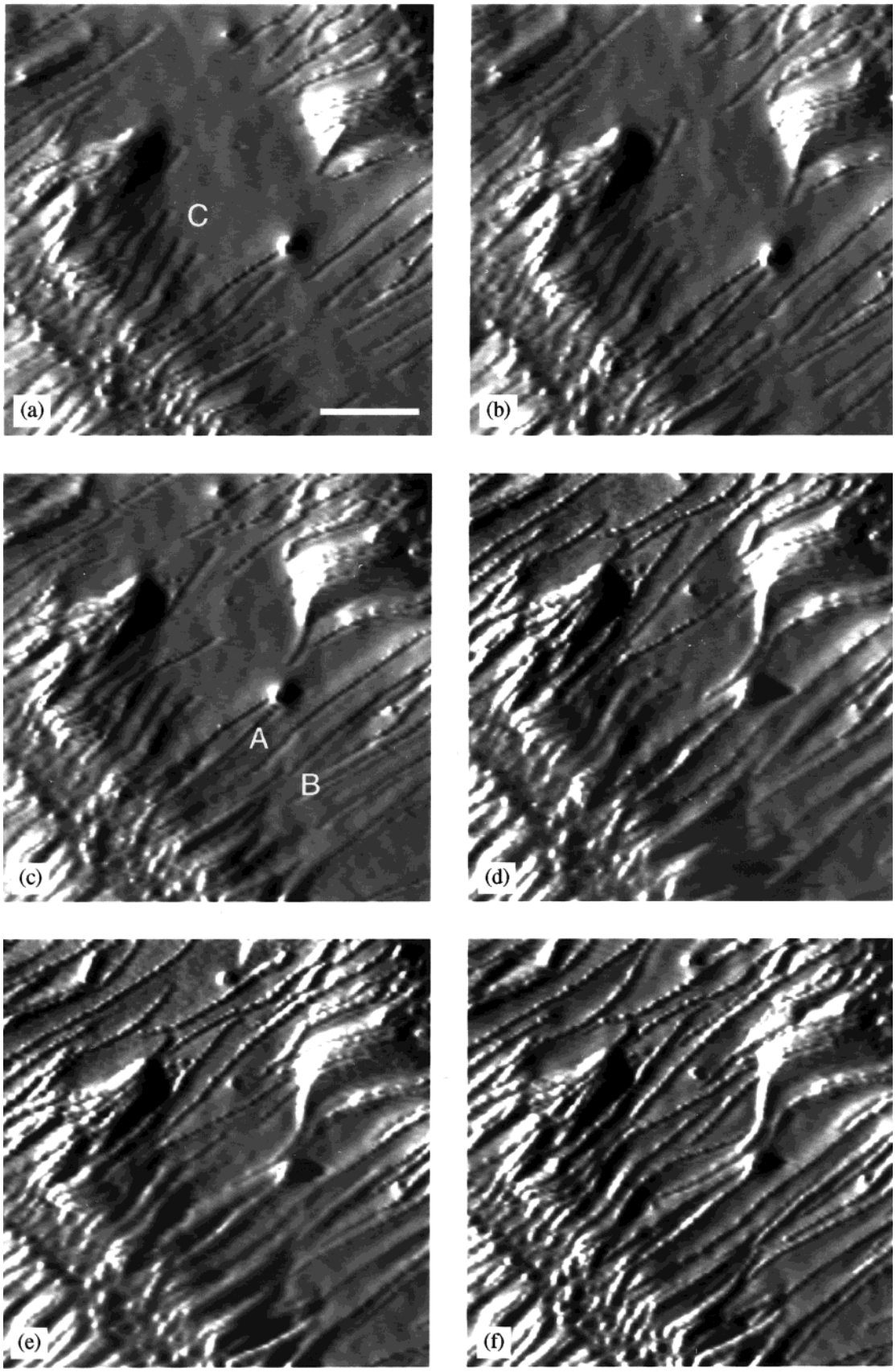

Figure 8. A series of amplitude images showing the interdigitation of two shish kebabs during cooling at 0.5 °C/min. The gray scale represents a change in amplitude of 0.3 V. The scale bar represents 300 nm. (a) Taken at 128.5 °C; the C shows a group of lamellae that, in subsequent images, can be seen to grow at different rates. (b) Taken at 127.9 °C. (c) Taken at 127.4 °C; the A shows a pair of lamellae that merge into one when they meet. The B shows a pair of lamellae that change direction to avoid meeting. (d) Taken at 125.7 °C. (e) Taken at 125 °C. (f) Taken at 123.9 °C.

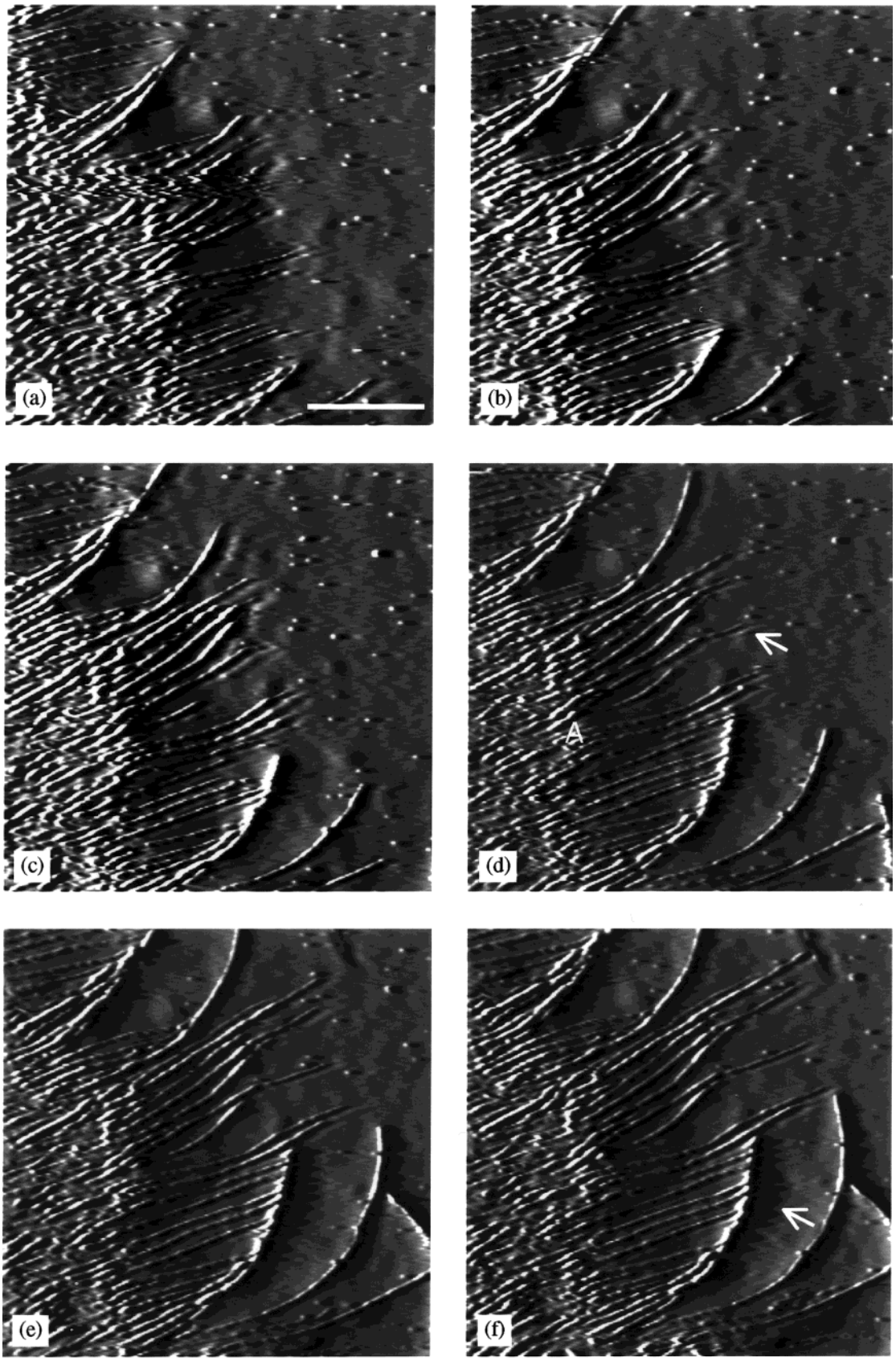

Figure 9. A series of amplitude images showing the isothermal growth of an oriented structure. The gray scale represents a change in amplitude of 1 V. The scan rate was 8.3 lines/s. The scale bar refers to all the images and represents 1 μm. (a) Taken at 0 s. (b) Taken at 152 s. (c) Taken at 275 s. (d) Taken at 465 s; the A indicates an infilling lamella. The arrow indicates an artifact caused by the fast scan speed, in which there appears to be an additional object next to the lamella. (e) Taken at 866 s. (f) Taken at 1204 s. The arrow indicates an artifact caused by the failure of the tip to track the surface after passing over a lamella.

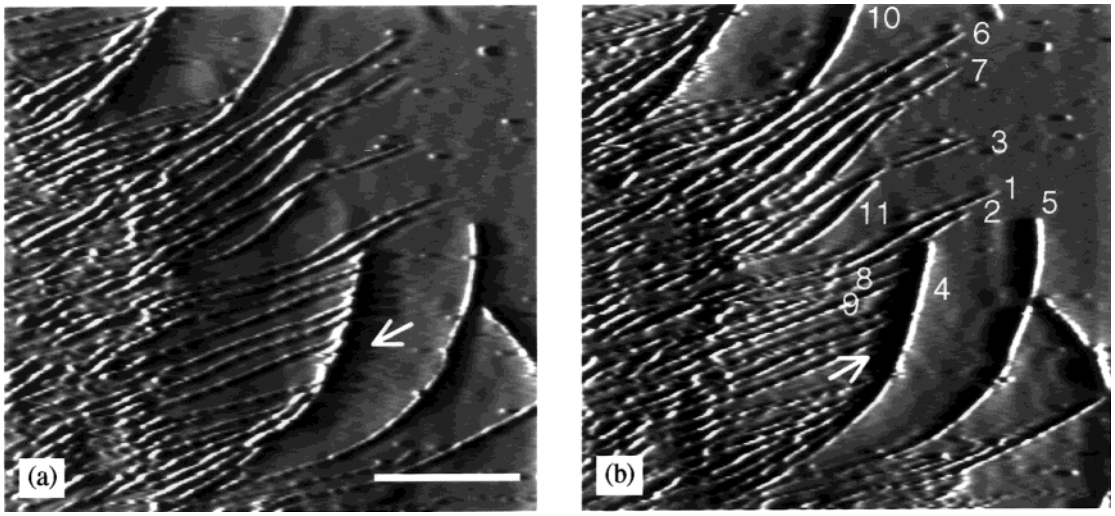

Figure 10. A pair of amplitude images collected on trace (a), and retrace (b), of the same scan. That is, the cantilever was moving from left to right in image (a) and from right to left in image (b). The gray scale represents a change in amplitude of 0.3 V. The scan rate was 8.3 lines/s. The scale bar represents 1 μm. The numbers indicate individual lamellae, the growth rates of which are shown in Figures 11 and 12. The arrows indicate the tracking artifact, caused by the feedback mechanism losing control as it passes over the higher object. These artifacts are on opposite sides of the lamella on scans in opposite directions.

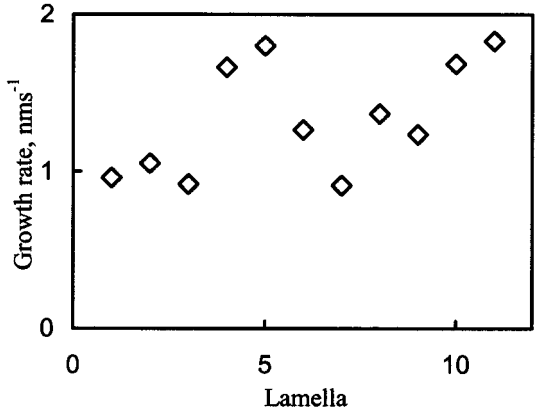

Figure 11. A graph showing the growth rate of the individual lamellae numbered in Figure 10, measured over ~278 s near the beginning of the experiment. Growth rates measured from the "trace" data.

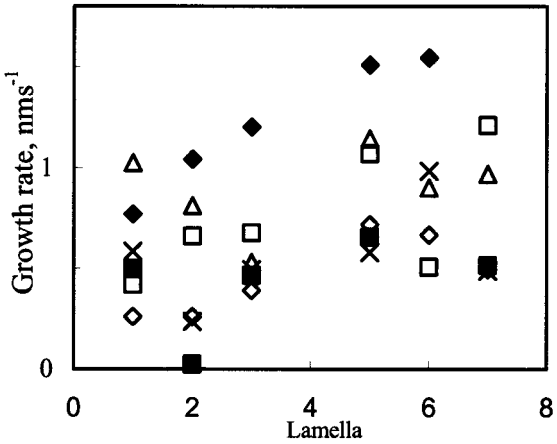

Figure 12. A graph showing the growth rate of the individual lamellae numbered in Figure 10 at different times during the experiment, taken from the retrace data: ◆, growth rate from the 10th to the 15th image of the series; □, growth rate from the 15th to the 20th image of the series; △, growth rate from the 20th to the 25th image of the series; ×, growth rate from the 25th to the 30th image of the series; ◇, growth rate from 30th to the 35th image of the series; ■, growth rate from the 35th to the 40th image of the series.

boring lamellae appear to have thickened to fill this available space, rather then a new lamella having crystallized.

Several possible reasons for this lack of nucleation suggest themselves. It may be that the crystallography of this particular part of the backbone is unfavorable to the nucleation of chain folded crystals and that if sufficient time had been allowed, nucleation would have occurred. Similarly, it may just be chance that no nucleus grew to a sufficient size to be stable before too much of the surrounding melt had been depleted by the growth of the neighboring lamellae. Alternatively, it may be that this 70 nm gap is not large enough to accommodate a new lamella, even though the actual crystal thickness that is growing is less than 30 nm; that is, it is necessary to have some particular amount of amorphous material surrounding a crystal as it grows. In all cases, there is a region of amorphous material on each side of the lamellae, so that the distance between next-nearest neighbors is typically ~100 nm. The presence of a characteristic amorphous thickness has been observed in ref 23 and used to support a new theory for polymer crystallization. In Figure 9 the growth of an "in-filling" lamella can be seen, labeled A. The gap between the lamellae into which this lamella is growing narrows slightly, to approximately 55 nm, and the in-filling lamella is not able to grow into this narrow gap. These observations support the view that both amorphous and crystal thicknesses are constrained by the crystallization conditions.

Interdigitation of Neighboring Shish Kebabs. As lamellae in two neighboring shish kebabs grow, they eventually start to overlap. It is this overlapping, and the interdigitation that sometimes occurs, that has been suggested to play an important role in the final properties of many oriented polymer articles.[7] Using standard techniques, it is not possible to learn much about this process, as the temperature and time at which each lamella crystallized are of crucial importance to an understanding of the process but are inaccessible using ex-situ methods. In Figures 4–6 and 8, the actual process of interdigitation can be followed. As two lamel-

lae approach each other, there are three different possible ways for the structure to develop. The two lamellae can just miss each other and pass by without having to change direction; they can hit each other and therefore stop growing; they can change their direction so as to avoid hitting each other. There are examples of all three types of behavior in the images shown here. Simply missing occurs frequently. There are a number of examples where two lamellae join, for instance labeled A in Figures 5c and 8c. In these cases the resultant, longer, lamella appears indistinguishable from a lamella that had grown as a single lamella, there is no sign of a join, and no further growth as the growth front has, presumably, been terminated.

The third of the above possibilities, namely that the lamellae change direction so as to avoid hitting each other, is the most interesting. Examples of this behavior can be seen in Figure 4c,d (labeled A), in Figure 5a,b (labeled B), and in Figure 8b,c (labeled B). The change in direction is very clear and occurs just before the two lamellae meet, resulting in a slight kink in one of the lamellae, a morphology that is sometimes visible in ex-situ examination of shish kebabs.[24] The change in direction of the lamella means that the presence of another crystal growing nearby influences the direction in which it grows, although the mechanism by which this occurs is unclear. Four possibilities present themselves:

i. During growth a slightly oriented zone is formed in front of the growing crystal, due to the volume reduction that occurs during crystallization and hence the "sucking in" of the polymer chains. As two oriented zones approach each other, molecules lying in between will be pulled in both directions and hence be stabilized compared to those lying further from the midpoint between the two lamellae. Thus, the oriented zones might tend to "deflect" each other, leading to the lamellae changing direction, as observed.

ii. As a lamella grows, either the melt must disentangle or the entanglements must migrate away from the growth front. It is likely that a combination of both processes occurs. If entanglements are pushed ahead of the growing crystal, there will be a region in front of each crystal that is particularly densely entangled and therefore difficult to crystallize. As a crystal grows, it will tend to take the path of least resistance, and thus such an entangled melt might act to repel the growth of an oncoming lamella.

iii. There may be a metastable region in front of the growing lamellae. These metastable regions might interact in some way so as enable the crystal to continue growing into the available melt.

iv. In a manner similar to (i) and (ii) above, there may be a buildup of impurities or other noncrystallizable material in front of the growing crystal, and these impurity-rich zones would tend to deter the joining together of opposing lamellae.

Explanations (iii) and (iv) above do not easily allow for the possibility that two approaching lamellae should join and become one, as is also frequently observed. As yet, we have not obtained sufficiently high-resolution images of this process of avoidance to be able to determine the mechanism. However, the fact that it is occurring, and the activity in the "melt" that it implies, is an additional piece of information that needs to be explicitly explained by any theory of polymer crystallization.

Growth Rates. As we have been able to obtain successive images of the same lamellae, it is possible to measure the lamellar growth rate. In the first two sets of experiments, Figures 3−8, the temperature was changed during crystallization, so the absolute rates are of little value. However, the comparison of growth rates of different lamellae, that is the extent to which the difference in length of different lamellae varies with time, is useful information. The older theories for polymer crystallization explicitly predict a constant lamellar growth rate at a particular temperature, on the scale of a few unit cells (i.e., a nanometer or so), as this was in agreement with the observation of constant growth rates when measured using optical microscopy, on a very different length scale. A number of AFM studies of lamellar scale growth have shown that the growth rate of individual lamellae often varies both from lamella to lamella and in time.[13,16,17] However, as the original theories were largely based on data from the crystallization of polyethylene, it is particularly instructive to look at the crystallization rates of this material. Indeed, the NBS fraction used here is one of the high molecular weight samples used in many of the studies of polyethylene growth.

It is immediately apparent that there is not one growth rate for the entire population of lamellae shown. First, a number of lamellae stop growing or never really start growing. In some cases the reason for this is clear. For instance, the lamella marked B in Figure 4 only grows until it hits the small spot in the image that is in front of it in Figure 4a. After this, the lamella lies dormant. The "spot", which is presumably an impurity of some sort, seems to have stopped the growth of the lamella. Also, in some cases the melt becomes so thin that depletion of material slows down or stops the growth of the crystals at the temperature of observation, examples of which can be seen as the edge where the melt meets the glass is approached by the growing crystals. This is a special case which only applies to very thin films, where a different, diffusion-limited type of growth is expected to dominate, so observations in these very thin parts of the film cannot be compared to the standard theories for polymer crystallization. In several other cases the lamellae grow very slowly, or stop growing, for no apparent reason. For instance, comparison of the lamella marked C in Figure 4d and the same lamella in Figure 6b (marked C there also) shows that very little growth has occurred.

There are also striking examples in these first two sets of experiments where the growth rate of an individual lamella varies with time. In Figure 8 three lamellae next to each other, marked C, grow at very different rates. Initially all three lamellae grow at the same rate. However, the upper one then changes direction slightly and starts to grow much faster, while its two neighbors stop growing. Finally, the two lower lamellae resume their growth. It seems that there is a mechanism that is poisoning the growth of some lamellae, in a manner similar to that already discussed at length in ref 13.

The crystallization process followed in Figure 9 was imaged at a nominally constant temperature, so the measurement of the actual growth rates is of more interest. Simply by observation of the images, it is immediately apparent that some of the lamellae grow faster than others. In particular, from Figure 11, all of the lamellae that are curved grow more rapidly, at least

at first. Indeed, these lamellae have the same radius of curvature of 1.2 μm. One possibility is that these crystals have their *b* axis in the direction of growth, while the other lamellae are otherwise oriented. As the *b* axis is the fast growth axis at this temperature, they will grow faster than the rest of the population. The curvature can then be explained by differences in fold surface structure, as suggested in ref 25 in which the formation of curved lamellae on crystallization in very thin films was observed. Another possibility is that the lamellae are able to curve because of lack of close neighbors, as has been suggested in ref 12, and maybe this then allows them to attain a faster growth rate. From inspection of Figure 12, it is clear that although the curved lamella, lamella 5 in this graph, grows faster at first, it does slow down to a rate similar to that of the rest of the lamellae. This slowing down occurs as it starts to approach lamella 1. Also, from Figure 12, the growth rate of lamella 6 is, at times, faster than the other straight growing lamellae. This is supporting evidence that the important factor affecting the growth rate is the proximity of other lamellae.

The growth rates of all the lamellae slow down slightly through the experiment. This is probably due to a slow approach to an equilibrium temperature that was slightly higher than the starting temperature, as the cantilever holder approaches the temperature of the heater. Superimposed on top of this slowing down are some other effects. All of the lamellae go through occasional spurts in growth. Also, if a lamella grows too close to an existing lamella, its growth rate slows down considerably, even though it would seem to be possible for them to grow along in parallel. Examples of this are lamella 11 and, toward the end of the experiment, lamella 2, which stops growing completely even though it does not actually hit another lamella.

It is very clear that the actual growth rates of the lamellae vary both from lamella to lamella, and with time for an individual lamella, both slowing down and speeding up. As this is a departure from the predictions of secondary nucleation theory, it is worthwhile exploring explanations for this behavior due to the particular experiment that we performed. A possible explanation for this is that the thickness of the film varies sufficiently to alter the diffusive barrier to crystallization. In the case of the experiment detailed in Figures 9−12, the film thickness only varies by a nanometer or so over a lateral distance of 100 nm, so it seems unlikely that this is having a significant impact. This degree of smoothness is typical for polyethylene films away from the substrate and before the crystallization itself has roughened the surface. The film in Figures 9−12 is slightly more than 100 nm thick, so we do not expect the film thickness to have a considerable impact on the growth rate, although the exact dependence of growth rate on film thickness in thin polyethylene films on a glass substrate is an area that has not been extensively explored in the literature, as, in very thin films, the observation of crystallization using techniques other than AFM is very difficult. If the growth rate in the area studied were being substantially suppressed by the film thickness, we would expect to have seen more extensive growth in the areas of the film that were thicker (when examining these areas optically and when doing lower resolution scans to ensure that the behavior in the region that we were imaging was typical). We did not see any such enhanced growth elsewhere, so will assume that the thickness of the film was not dominating the crystallization behavior. It is also possible that the observation of growth at the surface is in some way different from that in the rest of the film, perhaps due to a difference in mobility of the chains in the surface layer or a difference in the surface energies, and hence barrier to growth, when a free surface is present. If this were the case, we might expect to always see considerably enhanced growth at the surface, or some other similar effect, which has not been observed. We therefore do not think that it is unreasonable to assume that the behavior reported here is a novel result that needs to be explained by any complete theory for polymer crystallization.

It can be envisaged that when the rates are averaged, as would happen when observed optically, there is a temperature-dependent growth rate as is usually observed. However, this is not the instantaneous growth rate of the lamellae and is certainly not an indication of the true rate of growth on a crystallographic scale. Thus, theories, such as secondary nucleation theory, which predict a growth rate for a particular lamella, which would be a constant at a particular temperature and would only fluctuate over a few nanometers at most (that is, tens of stems), need modification to explain the data presented here. The total growth of the lamellae over the period of the experiment is only ∼1000 nm, so these data do not contradict the findings of optical microscopy; it is just studying the process at a different length scale. However, as secondary nucleation theory predicts the growth rate on a sublamellar length scale, i.e., the length scale that is being probed by this experiment, its predictions are contradicted.

Although this observation could have far-reaching implications for our understanding of polymer crystallization, we will leave a full discussion to a later paper where the data presented here can be combined with the compelling evidence of our studies on the crystallization of unoriented polyethylene structures.

Conclusions

A large volume of data has been presented showing, with unprecedented time and spatial resolution, the evolution and growth of polyethylene shish kebab structures. A number of observations with wide-reaching implications for our understanding of this industrially and scientifically important process have been made.

The meeting of opposing shish kebab crystals has been imaged, and new data on the process of interdigitation obtained which implies a strong influence on the melt, ahead of the advancing lamella, due to the crystallization process. The exact nature of this influence is as yet unclear.

The observation of parallel lamellae as they grow and nucleate from the extended backbone implies that it is necessary for there to be some minimum amount of amorphous material surrounding a lamella in order for it to grow.

By following the evolution of lamellae with time, growth rates have been obtained. These growth rates are found to vary both in time, for each lamella, and from lamella to lamella. This observation has wide-reaching implications for existing theories of polymer crystallization.

The direct observation of the process of crystallization in polyethylene, the paradigm for flexible chain crystal-

lization, without harming the sample and with high resolution, promises to revolutionize our understanding of this long studied material.

Acknowledgment. We thank the EPSRC for funding.

References and Notes

(1) Keller, A. *Philos. Mag.* **1957**, *2*, 1171.
(2) Keller, A. *Faraday Discuss. Chem. Soc.* **1979**, *68*, 45.
(3) Bassett, D. C. *Principles of Polymer Morphology;* Cambridge University Press: New York, 1981.
(4) Hoffman, J. D.; Frolen, L. J.; Ross, G. S.; Lauritzen, J. I. *J. Res. Natl. Bur. Stand. A: Phys. Chem.* **1975**, *79A*, 671.
(5) Lemstra, P. J.; van Aerle, N. A. J. M.; Bastiaansen, C. W. M. *Polym. J.* **1987**, *19*, 85.
(6) Keller, A. In *Ultrahigh Modulus Polymers;* Ciferri, A., Ward, I. M., Eds.; Applied Science Publishers: London, 1979; p 321.
(7) Odell, J. A.; Keller, A.; Miles, M. J. *Colloid Polym. Sci.* **1984**, *262*, 683.
(8) McHugh, A. J. *Polym. Eng. Sci.* **1982**, *22*, 15.
(9) Barham, P. J.; Keller, A. *J. Mater. Sci.* **1985**, *20*, 2281.
(10) Petermann, J.; Miles, M.; Gleiter, H. *J. Polym. Sci., Polym. Phys.* **1979**, *17*, 55.
(11) Lieberwirth, I.; Loos, J.; Petermann, J.; Keller, A. *J. Polym. Sci., Part B: Polym. Phys.* **2000**, *38*, 1183.
(12) Monks, A. W.; White, H. M.; Bassett, D. C. *Polymer* **1996**, *37*, 5933.
(13) Hobbs, J. K.; McMaster, T. J.; Miles, M. J.; Barham, P. J. *Polymer* **1998**, *39*, 2437.
(14) Pearce, R.; Vancso, G. J. *Polymer* **1998**, *39*, 1237.
(15) Schultz, J. M.; Miles, M. J. *J. Polym. Sci., Part B* **1998**, *36*, 2311.
(16) Vancso, G. J.; Beekmans, L. G. M.; Pearce, R.; Trifonova, D.; Varga, J. *J. Macromol. Sci., Phys.* **1999**, *B38* (5&6), 491.
(17) Li, L.; Chan, C.-M.; Yeung, K. L.; Li, J.-X.; Ng, K.-M.; Lei, Y. *Macromolecules* **2001**, *34*, 316.
(18) Godovsky, Y. K.; Magonov, S. N. *Langmuir* **2000**, *16*, 3549.
(19) Winkel, A. K.; Hobbs, J. K.; Miles, M. J. *Polymer* **2000**, *41*, 8791.
(20) Hobbs, J. K.; Miles, M. J. *Macromolecules* **2001**, *34*, 353.
(21) Han, W.; Lindsay, S. M.; Jing, T. *Appl. Phys. Lett.* **1996**, *69*, 4111.
(22) Hobbs, J. K.; Humphris, A. D. L.; Miles, M. J. Manuscript in preparation.
(23) Strobl, G. *Eur. Phys. J. E* **2000**, *3*, 165.
(24) Hobbs, J. K.; Miles, M. J. Manuscript in preparation.
(25) Keith, H. D.; Padden, F. J.; Lotz, B.; Wittmann, J. C. *Macromolecules* **1989**, *22*, 2230.

MA0104478